University of Birmingham

Improvement of a stochastic backscatter model and application to large-eddy simulation of street canyon flow

O'Neill, James; Cai, Xiaoming; Kinnersley, Robert

[Link to publication on Research at Birmingham portal](#)

Improvement of a stochastic backscatter model and application to large-eddy simulation of street canyon flow

J.J. O'Neill[a], X.-M. Cai[a]* and R. Kinnersley[b]

[a]School of Geography, Earth and Environmental Sciences, University of Birmingham, UK

[b]Environment Agency, Bristol, UK

*Correspondence to: X.-M. Cai, GEES, University of Birmingham, Edgbaston, Birmingham, B15 2TT. Email: x.cai@bham.ac.uk

Abstract

A stochastic backscatter (SB) subgrid-scale (SGS) model is applied, for the first time, to large-eddy simulation (LES) of street canyon flow. We model a 'skimming flow' regime under a neutrally stratified atmosphere, in which the approaching wind is perpendicular to the along-street axis of a street canyon of unity aspect ratio. Previous LESs of this type have shown an under-prediction the intensity of the primary eddy (PE) that forms within the street canyon, indicating a lack of momentum transfer across the roof-level shear layer. The SB model, however, acts to increase this momentum transfer, *bringing the simulated PE intensity significantly closer towards that observed in a corresponding wind-tunnel experiment*. A metric for the PE intensity, ω_{PE}, based on the two-dimensional vorticity field, is increased from around 70% of the wind-tunnel ω_{PE} value (with the Smagorinsky SGS model) to as much as 90% (with the SB model). Calculation of the air exchange rate at roof-level confirms that the rate of entrainment into the street canyon is increased with the inclusion of backscatter.

We also outline an improvement to the SB model prior to its application. In its previous version, a constraint on the magnitude of the backscatter acceleration variances ensured a

theoretically appropriate level of additional grid-scale (backscattered) energy. Here, a further constraint on the magnitude of the main covariance term also facilitates a *better representation of grid-scale vertical momentum flux*. This new constraint alone can help to increase the simulated ω_{PE} value by as much as 10% of the wind-tunnel ω_{PE} value, and requires almost no additional computational effort. The effect of varying the magnitude and length-scale of the imposed backscatter (via the backscatter coefficient and length of the filter used to generate the backscatter acceleration fields, respectively) is also investigated.

Keywords: Large-eddy simulation; Primary eddy; Skimming flow; Stochastic backscatter; Street canyon; Turbulence.

1. Introduction

Large-eddy simulation (LES) is well-equipped to model single-recirculation "skimming flow", where a largely isolated primary eddy (PE) forms within a street canyon of aspect ratio $H/W \approx 1$ (H is the building height, W the street width) when the mean wind is perpendicular to the street axis (Oke, 1987). Unlike the time-averaged RANS (Reynolds-averaged Navier-Stokes) modelling approach, used for such flows by, e.g., Baik and Kim (1999) and Jeong and Andrews (2002), LES is able to capture important unsteadiness in the roof-level turbulence field (Li *et al.*, 2006). The strengths of LES compared with RANS are also demonstrated in many other studies, e.g., Xie and Castro (2006), Dejoan *et al.* (2010), Tominaga and Stathopoulos (2010), Salim *et al.* (2011a) and Salim *et al.* (2011b), and. Liu and Barth (2002) were among the first to apply LES to an individual (reduced-scale) street canyon of unity aspect ratio; an analysis of subsequent driven scalar transport showed good agreement between predicted mean concentration profiles within the canyon and measured values. Soon after, Cui *et al.* (2004) conducted LES within a full-scale street canyon of unity aspect ratio. Mean normalised streamwise velocity (u), vertical velocity (w) and resolved-

scale turbulent kinetic energy (RS-TKE) profiles, generated at five locations across the canyon, gave a noteworthy reproduction of the main features observed in the corresponding wind-tunnel data of Brown *et al.* (2000). More recently, Cheng and Liu (2011) and Liu and Wong (2014) utilised larger computing resources to consider 3 and 12 adjacent street canyons, respectively, rather than the one canyon of Cui *et al.* (2004).

A shared deficiency amongst these LES modelling studies, however, is an under-prediction of the PE intensity within the street canyon. Since the background flow is typically prescribed above roof-level only, the total available momentum budget within the street canyon comes entirely from the free-stream flow above it; this deficiency thus indicates insufficient entrainment of high-momentum air across the roof-level shear layer. Given that LES is well validated in its representation of turbulence scales that are not too close to either the domain size or the grid resolution (Mason, 1994), it is likely that the LES models are failing to accurately represent either (or both) the large-scale eddies within the free-stream flow that bring momentum into the street canyon via large 'sweep' events (Inagaki *et al.*, 2012), or the small (grid-scale and below) eddies within the roof-level shear layer that mix momentum down into the street canyon via turbulent diffusion (Letzel *et al.*, 2008). The LES domain size limits the size of the large-scale eddies in the free-stream flow; their vertical extent is restricted by the domain lid height and their horizontal extent confined to half the domain width (assuming periodic lateral boundary conditions). Interestingly, however, Cheng and Liu (2011) and Liu and Wong (2014) observed no significant change in their normalised velocity profiles (and, by inference, in their simulated PE intensity) compared with Cui *et al.* (2004), despite modelling more than one adjacent street canyon (the domain size was also increased in the span-wise and vertical directions). This will have allowed for significantly larger free-stream eddies to form, which suggests that a significant portion of their simulation degradation was attributable to the misrepresentation of the grid-scale (and smaller) eddies.

Improving simulation accuracy of the smaller turbulence scales at roof-level is a challenging task. In this region, a narrow shear layer exists due to the sharp reduction in streamwise velocity between the fast-moving free-stream air above the street canyon and the relatively slow-moving air within it. Within this shear layer, small (yet energetic) eddies are continually generated through Kelvin-Helmholtz instability (Louka *et al.*, 2000). Very fine grid spacing is therefore required in order to explicitly resolve much of this roof-level turbulence. The LES simulations performed by Letzel *et al.* (2008) suggest that a resolution of at least 100 across-canyon grid points is required in order to explicitly resolve these Kelvin-Helmholtz waves. However, their associated large computational demands necessitated a rather low domain lid height of only $1.5H$. Indeed, the computational resources available to most industrial end-users are typically far smaller than those available to research institutions, and resolution sacrifices are often unavoidable.

In the majority of cases, then, limited computational resources will necessitate the treatment of a significant portion of this roof-level turbulence by the LES model's subgrid-scale (SGS) parametrization scheme. The under-prediction of the PE intensity in the aforementioned LES studies suggests that the SGS models used are over-dissipative (i.e. have excessively large SGS viscosities), leading to a lack of turbulent mixing between the free-stream air above and the air within the street canyon (i.e. through the roof-level shear layer). The SGS models used included: the dynamic model (Germano *et al.*, 1991), adopted by Liu and Barth (2002); the Smagorinsky (1963) model, adopted by Cui *et al.* (2004) and; the one-equation model (Schumann, 1975), adopted by Cheng and Liu (2011) and Liu and Wong (2014).

We note that none of these SGS models are able to directly model the effects of backscatter; that is, the transfer of energy from the unresolved (subgrid) to the smallest resolved (grid) scales. In theory, dynamic models may consider backscatter by imposing locally negative eddy-viscosity values; however, in practice, negative values are typically prohibited to avoid

numerical instability, e.g. Basu and Porte-Agel (2006). In their paper on SGS modelling for LES of the horizontally homogeneous neutral atmospheric boundary layer (ABL), Mason and Thomson (1992) discuss how backscatter is most significant in regions of the flow where small (grid-scale) but energetic eddies are present. Such eddies are also present at the street canyon roof level (which, like the neutral ABL case, involves a strong shear layer), and backscattered energy is thus also likely to be large here. It is therefore worth testing whether a SGS model that can model backscatter directly could help to improve the simulation accuracy of street canyon flow. In the same paper, Mason and Thomson proposed a stochastic SGS modelling approach, in which the effects of backscatter are explicitly modelled by imposing pseudo-random accelerations on top of the LES acceleration field obtained with the Smagorinsky model. Although this stochastic backscatter (SB) model was based more on physical and dimensional reasoning than theoretical rigour, in practice it was shown to be highly effective in improving modelled statistics (particularly mean velocity shear) within the neutral surface layer. Similar improvements were also achieved with later revised versions of this SB model for application to the stable ABL (Brown *et al.*, 1994) and the dry convective ABL (Weinbrecht and Mason, 2008). A stochastic approach to modelling backscatter has also been used to improve simulation accuracy at other atmospheric scales, including at the mesoscale to improve forecast skill (Shutts, 2005, Palmer *et al.*, 2009), and in general circulation models to improve simulated energy spectra (Zidikheri and Frederiksen, 2009).

The performance of a given SB model may be judged by how successfully it matches modelled statistics of the grid-scale turbulence field with observed statistics; this will typically depend on the number of physical constraints imposed on the backscatter fields. Originally, Mason and Thomson (1992) imposed that their backscatter acceleration fields should be divergence-free – thus ensuring that the adjusted LES fields continue to satisfy mass conservation – and that the sum of the three acceleration variance components, which

relates directly to the imparted backscattered energy, should be appropriately spatially scaled. More recently, O'Neill *et al.* (2015) proposed a modification to this SB model to ensure that the backscatter length-scale ('eddy size') and level of anisotropy ('eddy shape') could be varied in conjunction with the locally expected length-scale and anisotropy of the grid-scale turbulence field (based, for example, on empirical observations), thus avoiding previous grid-dependency issues whilst also providing a more versatile alternative to the modification of Weinbrecht and Mason (2008).

In this paper, we propose a further modification to the SB model of O'Neill *et al.* (2015), designed to improve the representation of grid-scale vertical momentum flux (section 2). We then test the improved SB model in a simulation of flow within a street canyon of unity aspect ratio: section 3 describes the wind-tunnel dataset used for model validation, as well as the configuration of the LES and SB models; section **Error! Reference source not found.** presents the results and provides discussion. Finally, conclusions are drawn and future work is outlined in section 5.

2. Improving the stochastic backscatter model

In this section, we outline an improvement to the SB model of O'Neill *et al.* (2015). This improvement allows the grid-scale vertical momentum flux, which affects the rate of entrainment through the shear-layer and is thus potentially important to the simulated primary eddy intensity, to be adjusted towards a level that is more representative of, for example, empirical observations. Importantly, this modification does not affect the ability of the model to satisfy its other constraints, and requires almost no additional computational effort. We also stress that this modification can be used to improve the representation of backscatter in any general two-dimensional shear flow in which two of the three momentum flux

components are virtually zero, i.e. it is not solely applicable to the present case of street canyon flow.

As detailed in O'Neill *et al.* (2015), the SB model uses random acceleration fields, $\boldsymbol{a}$, that continually augment the LES acceleration field, to represent the apparent stochastic effects of backscatter from the unresolved to the resolved scales:

$$\frac{\partial u_i}{\partial t} = \cdots + \frac{\partial}{\partial x_j}\left\{ v_{\text{sgs}}\left(\frac{\partial u_i}{\partial x_j} + \frac{\partial u_j}{\partial x_i}\right)\right\} + a_i, \tag{1}$$

sum over $j = 1,2,3$, where $u_i = \{u, v, w\}$ is the LES (filtered) velocity field, t is time, $x_i = \{x, y, z\}$ is a Cartesian coordinate system, v_{sgs} is a subgrid-scale eddy-viscosity obtained using the Smagorinsky model, and the ellipsis signifies all other adopted terms from the filtered Navier-Stokes equations.

These acceleration fields are generated by taking the curl of a random vector potential $\boldsymbol{\phi}$, i.e. $\boldsymbol{a} = \nabla \times \boldsymbol{\phi}$, which ensures zero divergence. The vector potential itself is the product of two fields; $\boldsymbol{\phi} = g\widehat{\boldsymbol{\phi}}$, where $\widehat{\boldsymbol{\phi}}$ is a (spatially filtered) random vector field with zero mean and unit variance, and g is a scalar field that ensures the appropriate local energy backscatter rate (which is a function of the local dissipation rate, ϵ, following the theory of Mason and Thomson (1992)). The three component (scalar) fields of $\widehat{\boldsymbol{\phi}}$ in the x, y and z dimensions are denoted by $\hat{\phi}_x$, $\hat{\phi}_y$ and $\hat{\phi}_z$, respectively. We also define $\hat{\phi}_1$, $\hat{\phi}_2$ and $\hat{\phi}_3$ as three *independently generated* random scalar fields, each with zero mean and unit variance. With the previous version of the SB model in O'Neill *et al.* (2015), each component field of $\widehat{\boldsymbol{\phi}}$ is taken to be independent of the others, i.e.:

$$\{\hat{\phi}_x, \hat{\phi}_y, \hat{\phi}_z\} = \{\hat{\phi}_1, \hat{\phi}_2, \hat{\phi}_3\}, \tag{2}$$

In this study, we also consider an alternative approach in which the first and third component fields can be correlated with each other, i.e.:

$$\{\hat{\phi}_x, \hat{\phi}_y, \hat{\phi}_z\} = \{\hat{\phi}_1, \hat{\phi}_2, \alpha\hat{\phi}_1 + \sqrt{1-\alpha^2}\hat{\phi}_3\}, \quad \text{where} \quad 0 \leq \alpha \leq 1 \tag{3}$$

This formulation ensures that $\hat{\phi}_z$ always has unit variance. Thus, when $\alpha = 0$, $\hat{\phi}_z$ is fully independent of $\hat{\phi}_x$ and we retrieve the original approach given by Eq. (2); when $\alpha = 1$, $\hat{\phi}_x$ and $\hat{\phi}_z$ are identical. For intermediate values of α, $\hat{\phi}_x$ and $\hat{\phi}_z$ will be correlated to some degree.

To understand why this may be useful from the point of view of controlling grid-scale vertical momentum flux, we first require a way to link the effect of the backscatter *accelerations* on the LES *velocity* fields. We first note that the backscatter time-scale, T_B, i.e. the time between the generation of each new (independent) backscatter acceleration field, is necessarily small (on the order of the model time-step, Δt) in order to ensure that all fluid elements experience the same time-scale of stress variation (Mason and Brown, 1994). We may thus linearly approximate the backscatter velocity fluctuations (which we denote by subscript B) from the backscatter accelerations as $u'_{i_B} = a_i T_B$, where $u'_{i_B} \equiv u'_B, v'_B, w'_B$ for $i = 1,2,3$ represent fluctuations in x, y and z respectively. The six (independent) components of the resulting stress tensor relating to the backscatter velocity fluctuations, $\overline{u'_i u'_j}_B$, (where the overbar denotes a time average) are thus well approximated by:

$$\begin{bmatrix} \overline{u'^2}_B & \overline{u'v'}_B & \overline{u'w'}_B \\ & \overline{v'^2}_B & \overline{v'w'}_B \\ & & \overline{w'^2}_B \end{bmatrix} = T_B^2 \begin{bmatrix} \overline{a_1^2} & \overline{a_1 a_2} & \overline{a_1 a_3} \\ & \overline{a_2^2} & \overline{a_2 a_3} \\ & & \overline{a_3^2} \end{bmatrix} \tag{4}$$

It follows from the backscatter acceleration field generation procedure (see Appendix A for a more detailed derivation) that the local magnitude of each of these six terms is well approximated by:

$$\overline{u'^2}_B = 2T_B^2 g_{i,j,k}^2 \left[\left(1 - \rho_{i,j,k}^{\Delta y_j}\right)/\Delta y_j^2 + \left(1 - \rho_{i,j,k}^{\Delta z_k}\right)/\Delta z_k^2\right]$$

$$\overline{v'^2}_B = 2T_B^2 g_{i,j,k}^2 \left[\left(1 - \rho_{i,j,k}^{\Delta z_k}\right)/\Delta z_k^2 + \left(1 - \rho_{i,j,k}^{\Delta x_i}\right)/\Delta x_i^2 - \underline{\alpha\left(1 - \rho_{i,j,k}^{\Delta x_i} - \rho_{i,j,k}^{\Delta z_k} + \rho_{i,j,k}^{\Delta x_i}\rho_{i,j,k}^{\Delta z_k}\right)/\Delta x_i \Delta z_k}\right]$$

$$\overline{w'^2}_B = 2T_B^2 g_{i,j,k}^2 \left[\left(1 - \rho_{i,j,k}^{\Delta x_i}\right)/\Delta x_i^2 + \left(1 - \rho_{i,j,k}^{\Delta y_j}\right)/\Delta y_j^2\right]$$

$$\overline{u'v'}_B = -T_B^2 g_{i,j,k}^2 \left[\left(1 - \rho_{i,j,k}^{\Delta x_i} - \rho_{i,j,k}^{\Delta y_j} + \rho_{i,j,k}^{\Delta x_i}\rho_{i,j,k}^{\Delta y_j}\right)/\Delta x_i \Delta y_j - \underline{\alpha\left(1 - \rho_{i,j,k}^{\Delta y_j} - \rho_{i,j,k}^{\Delta z_k} + \rho_{i,j,k}^{\Delta y_j}\rho_{i,j,k}^{\Delta z_k}\right)/\Delta y_j \Delta z_k}\right]$$

$$\overline{u'w'}_B = -T_B^2 g_{i,j,k}^2 \left[\underline{2\alpha\left(1 - \rho_{i,j,k}^{\Delta y_j}\right)/\Delta y_j^2} + \left(1 - \rho_{i,j,k}^{\Delta x_i} - \rho_{i,j,k}^{\Delta z_k} + \rho_{i,j,k}^{\Delta x_i}\rho_{i,j,k}^{\Delta z_k}\right)/\Delta x_i \Delta z_k\right]$$

$$\overline{v'w'}_B = -T_B^2 g_{i,j,k}^2 \left[\left(1 - \rho_{i,j,k}^{\Delta y_j} - \rho_{i,j,k}^{\Delta z_k} + \rho_{i,j,k}^{\Delta y_j}\rho_{i,j,k}^{\Delta z_k}\right)/\Delta y_j \Delta z_k - \underline{\alpha\left(1 - \rho_{i,j,k}^{\Delta x_i} - \rho_{i,j,k}^{\Delta y_j} + \rho_{i,j,k}^{\Delta x_i}\rho_{i,j,k}^{\Delta y_j}\right)/\Delta x_i \Delta y_j}\right]$$

$$(5)$$

where subscripts i, j and k now denote the three discrete model grid-point indices in x, y and z, respectively, Δx, Δy and Δz are the local grid spacings, and $\rho^{\Delta \zeta}$ is the auto-correlation coefficient between two adjacent grid points in the ζ dimension within any of the three $\hat{\phi}$ fields (the local value will be the same for each field, since the same filtering procedure is applied to each of $\hat{\phi}_1$, $\hat{\phi}_2$ and $\hat{\phi}_3$).

The underlined terms in Eq. (5) show the additional terms that appear as a result of using Eq. (3) over Eq. (2). If we choose to adopt the same spatial filtering procedure on the $\hat{\phi}$ fields with the old and new approaches (meaning that all $\rho^{\Delta \zeta}$ values remain unchanged from one approach to the other), we see that, with the new approach, the magnitude of the backscatter covariance component $\overline{u'w'}_B$ is increased (by an amount which depends on the value of α), and the magnitude of the $\overline{u'v'}_B$ and $\overline{v'w'}_B$ components are reduced (by a smaller amount). Furthermore, the auto-variance component $\overline{v'^2}_B$ is also slightly reduced, and, since the sum of the three auto-variance components is fixed by the locally expected energy backscatter rate, components $\overline{u'^2}_B$ and $\overline{w'^2}_B$ must therefore also increase slightly. Before analysing more formally how strongly each term is altered for varying values of α, we first consider the

expected magnitudes of the Reynolds stresses, $\overline{u_i' u_j'}$, within the roof-level shear layer from a theoretical and empirical perspective.

For a two-dimensional (2-D) mean flow such as the one presently considered, we expect everywhere velocity fluctuations in the homogeneous direction (here, the spanwise, or along-street, direction) to be uncorrelated with velocity fluctuations in the other two directions (here, the streamwise and vertical directions), i.e. $\overline{u'v'}$, $\overline{v'w'} = 0$ (with the y-axis aligned along the street). The $\overline{u'w'}$ component, however, will be non-zero and thus represents the total vertical momentum flux. Hinze (1972) provided a full derivation of the dynamic equation for $\overline{u'w'}$ in an incompressible steady-mean shear flow. The shear layer at street canyon roof-level represents a plane mixing layer, formed at the boundary of two co-directional flows of differing speeds (Letzel *et al.*, 2008), and is characterised experimentally by a narrow peak in TKE and $\overline{u'w'}$ measurements at that height, e.g. Louka *et al.* (2000), Blackman *et al.* (2015). Louka *et al.* (2000) analysed the TKE budget equation for neutral flow to reveal that this peak in $\overline{u'w'}$ is a result of a maximum in the shear-production term at roof-level.

In light of the above, we also allow the backscatter stress term $\overline{u'w'}_{\mathrm{B}}$ to be non-negligible within the roof-level shear-layer region. We define a new parameter called the 'backscatter vertical momentum flux factor', $\mathrm{VMF}_{\mathrm{B}}$, which describes the ratio of the magnitude of $\overline{u'w'}_{\mathrm{B}}$ to $\sigma_{u\mathrm{B}} \sigma_{w\mathrm{B}}$, where, e.g., $\sigma_{u\mathrm{B}} \equiv \sqrt{\overline{u'^2}_{\mathrm{B}}}$:

$$\mathrm{VMF}_{\mathrm{B}} = \frac{\left| \overline{u'w'}_{\mathrm{B}} \right|}{\sigma_{u\mathrm{B}} \sigma_{w\mathrm{B}}}. \tag{6}$$

Substituting in the corresponding terms from Eq. (5) and rearranging for α, we get:

$$\alpha_{i,j,k} = \frac{2\,\text{VMF}_\text{B}\sqrt{\left[\frac{\left(1-\rho_{i,j,k}^{\Delta y_j}\right)}{\Delta y_j^2} + \frac{\left(1-\rho_{i,j,k}^{\Delta z_k}\right)}{\Delta z_k^2}\right]\left[\frac{\left(1-\rho_{i,j,k}^{\Delta x_i}\right)}{\Delta x_i^2} + \frac{\left(1-\rho_{i,j,k}^{\Delta y_j}\right)}{\Delta y_j^2}\right] - \frac{1-\rho_{i,j,k}^{\Delta x_i} - \rho_{i,j,k}^{\Delta z_k} + \rho_{i,j,k}^{\Delta x_i}\rho_{i,j,k}^{\Delta z_k}}{\Delta x_i \Delta z_k}}}{\frac{2\left(1-\rho_{i,j,k}^{\Delta y_j}\right)}{\Delta y_j^2}}. \tag{7}$$

We note that the permissible range of VMF_B is limited by α; the minimum value corresponds to when $\alpha = 0$ and the maximum value to when $\alpha = 1$.

We demonstrate the new approach more formally with an example of its application. For simplicity, we consider an isotropic model grid with resolution Δ, and the use of a discrete Gaussian filter with a width (or 'backscatter length-scale') of $l_\text{B} = \Delta$ when filtering each $\hat{\phi}$ field, which results in an auto-correlation coefficient of $\rho^\Delta = 0.8$ everywhere and (with the old approach) fully isotropic backscatter. We normalise the resulting backscatter stresses by the sum of the three auto-variance components, which is fixed for a given dissipation field. The resulting (relative) magnitudes are shown in Figure 1 for the cases: (a) $\alpha = 0$ (equivalent to the old approach in which $\hat{\phi}_x$ and $\hat{\phi}_z$ are fully independent), which corresponds to a value of $\text{VMF}_\text{B} = 0.05$, and; (b) $\text{VMF}_\text{B} = 0.5$ (i.e. $\hat{\phi}_z$ and $\hat{\phi}_x$ are correlated to such a degree that the magnitude of $\overline{u'w'}_\text{B}$ is half that of $\sigma_{u\text{B}}\sigma_{w\text{B}}$), which corresponds to a value of $\alpha = 0.89$. We see that with the old approach, all three covariance components are very small compared with the auto-variance components (around 5% the size). No consideration was previously given to the magnitude of the covariance components; they were simply a by-product of the overall backscatter generation procedure. With the new approach, we see that by increasing VMF_B (i.e. making $\hat{\phi}_x$ and $\hat{\phi}_z$ more correlated), the magnitude of the $\overline{u'w'}_\text{B}$ component relative to the three auto-variance components can be increased significantly. The maximum achievable value of VMF_B (corresponding to $\alpha = 1$) is approximately 0.6 in this case. The other two covariance components, $\overline{u'v'}_\text{B}$ and $\overline{v'w'}_\text{B}$, tend to zero as α tends to 1. We note that because

the auto-variance component $\overline{v'^2}_B$ is slightly reduced (and consequently $\overline{u'^2}_B$ and $\overline{w'^2}_B$ slightly increased) with the new approach, we have sacrificed a small amount of accuracy in our intention to generate fully isotropic backscatter acceleration fields. However, even with the maximum value of VMF_B (when $\alpha = 1$) , this reduction is not large ($\overline{v'^2}_B$ is only around 10% smaller than the other two auto-variance components). Note also that the backscatter acceleration fields can still be scaled such that the sum of the three auto-variance components remains at the intended value, and so we do not violate the intended local energy backscatter rate.

3. Experimental Design

A LES model is configured, with the SB model, to simulate flow within a full-scale street canyon of aspect ratio $H/W = 1$, such that model output can be compared against data from an equivalent (smaller-scale) wind-tunnel experiment. The wind-tunnel dataset is described in section 3.1, the LES model configuration in section 3.2, and the SB model configuration in section 3.3.

3.1. Wind-tunnel data

This wind-tunnel experiment, conducted by Brown *et al.* (2000), consisted of six adjacent 'street canyons' formed by seven solid rectangular blocks, each measuring $0.15 \text{ m} \times 0.15 \text{ m} \times 3.8 \text{ m}$, placed with their long face perpendicular to the oncoming wind direction x and spaced equally apart to form street canyons of unity aspect ratio. Among other variables, the mean streamwise and vertical velocity components (u and w) and the turbulence intensity were calculated from high-temporal-resolution measurements taken at various heights along five separate transects within the furthest-downwind (i.e. the sixth) street canyon. Each transect was at a different along-width location, namely at $x/W = -0.4, -0.12, 0, 0.25$ and 0.4, where $x = 0$ corresponds to the street canyon centre-point. Measurements from the last

street canyon best represent the equilibrium flow regime observed in the limit of an infinite number of canyons, which is arguably of greater interest than the flow regime observed in more isolated street canyons, since large urban areas often consist of many such repeating 'blocks' of buildings.

3.2. LES configuration

The LES modelling domain is schematised in Figure 2. The street canyon has dimensions $H = W = 18$ m, making it 120 times larger than the wind-tunnel street canyon. Full-scale experimental datasets of high enough quality to validate LES model output are lacking due to the difficulties associated with controlling the external conditions in such experiments. Consequently, many wind tunnel experiments have been conducted using similar block sizes to Brown *et al.* (2000) for the purpose of assessing the mixing of momentum and scalars in street canyon flow, e.g. Pavageau and Schatzmann (1999), Kastner-Klein and Plate (1999), Salizzoni *et al.* (2009), and subsequently used for validation purposes in full-scale numerical studies, e.g. Walton and Cheng (2002), Cui *et al.* (2004), Letzel *et al.* (2008), Cai *et al.* (2008). The x (across-canyon), y (along-canyon) and z (vertical) extent of the domain are $L_x, L_y, L_z = 24$ m, 40 m, 94 m, respectively. The open boundaries in x and y are treated as periodic, implying an infinitely long (repeating) canyon in y and an infinite number of repeated street canyons in the streamwise direction. Constant grid spacings of $\Delta x = 0.3$ m and $\Delta y = 1$ m are used in the streamwise and spanwise directions, respectively. The number of grid points in each of these directions is thus $N_x = 81$ and $N_y = 40$, respectively. In the vertical direction, there are $N_z = 91$ grid levels; a constant grid spacing of $\Delta z = 0.3$ m is used between the ground and $z/H = 1$, and Δz is then gradually stretched such that $\Delta z = 5$ m by the top of the domain.

The initial wind profile is logarithmic, starting from zero at the street canyon roof level (velocities are zero within the canyon) and reaching a maximum of 2.6 m s^{-1} at the domain lid.

A rough-wall boundary condition is used at solid surfaces, with normal velocities set to zero and tangential velocities based on a logarithmic profile. The use of a smooth-wall boundary condition, which would require a grid resolution fine enough to resolve up to the viscous sublayer, is unfeasible for atmospheric (high Reynolds number) flows. Although the need for better rough-wall models in simulations of complex flows such as the one presently considered is recognised within the LES community (Piomelli and Balaras, 2002), the logarithmic wall function is still, to our knowledge, the best and simplest choice available for rough walls, and widely adopted by numerous LES studies of flows over building-like obstacles in the past, e.g. Santiago *et al.* (2010), Park and Baik (2013), Cheng and Porte-Agel (2015).

The baseline Smagorinsky SGS model uses a fixed coefficient of $C_S = 0.1$. Mason and Callen (1986) reported that this value gives optimum behaviour in practical simulations of neutral flow, and that values as large as the theoretical one for homogeneous isotropic turbulence (Lilly, 1967) give excessive damping of the resolved scale motions. A number of LES studies of neutrally stratified flows have adopted similar values for the Smagorinsky constant, e.g. Xie *et al.* (2004), Santiago *et al.* (2010), Boppana *et al.* (2010).

The present LES model was developed by Cui *et al.* (2004) and is based on Colorado State University's Regional Atmospheric Modelling System (RAMS), originally developed by Pielke *et al.* (1992). The dynamic core of RAMS is scale independent; it adopts the finite volume method to solve the non-hydrostatic equations on a staggered Arakawa-C grid, using a flux conservative leapfrog time differencing method and with 2nd order spatial accuracy. A model time-step of $\Delta t = 0.04$ s is used.

All simulations are run to a time of 75 minutes, which corresponds to around 25 turnover times of the primary eddy within the street canyon, with data from the last 15 minutes of each

simulation used to calculate average flow statistics. As the mean flow field is 2-D, data are also averaged in the homogeneous spanwise (y) direction.

3.3. Stochastic backscatter model configuration

Following the theory of Mason and Thomson (1992), away from surfaces we should scale the backscatter acceleration fields such that

$$\overline{a_1^2} + \overline{a_2^2} + \overline{a_3^2} = \frac{2C_{\text{B}}}{T_{\text{B}}}\epsilon, \tag{8}$$

where C_{B} is the backscatter coefficient, which typically takes a value within the range $0.6 - 1.4$ (Chasnov, 1991, Mason and Thomson, 1992, Weinbrecht and Mason, 2008). In our analysis, we shall test three different values for the backscatter coefficient that cover this range; namely $C_{\text{B}} = 0.6, 1.0$ and 1.4. We note that Mason and Thomson's original analysis was based on neutrally stratified flow with a high Reynolds number (Re); we assume a sufficiently high Re in the current street canyon case for the grid-scale backscatter to be unaffected by the change in scale.

We use $T_{\text{B}} = 2\Delta t$ as the backscatter time-scale, i.e. a new backscatter acceleration field is generated every other model time-step. As discussed by Mason and Brown (1994), although a more realistic treatment of this time-scale is possible, a value of T_{B} on the order of the model time-step removes the need for Lagrangian-type following of fluid elements.

Where possible, it is sensible for computational efficiency to apply the backscatter accelerations only in regions of the flow where ϵ (and therefore the energy backscatter rate) is large. Here, we shall confine our attention to the region of the energetic roof-level shear layer only. Horizontally-averaged (denoted by angled brackets) and time-averaged vertical profiles of the dissipation rate, $\langle\overline{\epsilon}\rangle$, (not shown) reveal a peak at roof-level that drops off sharply in both directions such that $\langle\overline{\epsilon}\rangle$ is at least a factor of 10 smaller by $z = 0.8H$ and

$z = 1.2H$. We thus only apply the backscatter accelerations within this bounded region, i.e. within $0.8 \leq z/H \leq 1.2$ (as indicated by the shaded region in the schematic Figure 2). Figure 3(a) also shows an x-z contour slice through this region for an instantaneous dissipation field, which provides an example of the typically sharp drop-off in ϵ from roof-level.

To determine the shape of the grid-adaptive filter (GAF) used in the backscatter generation procedure of O'Neill *et al.* (2015), the local backscatter length-scale, l_B, and level of anisotropy must be predefined. Clearly, since the aim of the SB model is to model backscatter from the unresolved to the smallest resolved scales, l_B should be on the order of the local LES-filter scale, which is typically assumed to be on the order of the local grid-scale. However, in finite-difference LES codes that use anisotropic and/or variable grid spacing, ambiguity exists over the effective local grid resolution. The geometric mean of the three local grid spacings in each dimension is one often-used measure (Deardorff, 1970); we might thus define the local backscatter length-scale as

$$l_B = \left(\Delta x_i \Delta y_j \Delta z_k \right)^{1/3}, \tag{9}$$

Alternatively, Mason and Brown (1999) suggest that the effective grid resolution is governed by the coarsest of the three local grid spacings; we might thus instead define the local backscatter length-scale as

$$l_B = \max\{ \Delta x_i, \Delta y_j, \Delta z_k \}, \tag{10}$$

For our analysis, we shall test both these definitions for l_B. For the LES model grid used in this study, Eq. (9) gives $l_B = 0.45$ m below roof-level (where $\Delta z = 0.3$ m) and Eq. (10) gives $l_B = 1$ m. For simplicity, we choose to impose fully isotropic backscatter acceleration fields in this study, i.e. we assume that $\overline{a_1^2} = \overline{a_2^2} = \overline{a_3^2}$ everywhere, however we note that the imposition of anisotropic backscatter is also possible with the SB model.

We note that a point-wise scaling factor must be used when scaling the backscatter acceleration fields, as opposed to the vertical scaling factor used in the neutral ABL simulations in O'Neill *et al.* (2015), since the street canyon turbulence field is not horizontally homogeneous. As done in previous studies (Mason and Thomson, 1992, Weinbrecht and Mason, 2008), we filter the instantaneous dissipation field prior to the calculation of the expected point-wise energy backscatter rates (Eq. (8)) to ensure that variations in ϵ occur on a similar spatial scale to variations in the backscatter accelerations. To do this, we simply apply the same filter used on the $\hat{\phi}$ fields during the backscatter generation procedure to the ϵ field, with the key difference that the filter weights are normalised (i.e. scaled to sum to unity at each grid point) to ensure that ϵ is conserved. Figure 3 demonstrates the effect of filtering the dissipation field in this way (where $l_B = \left(\Delta x_i \Delta y_j \Delta z_k\right)^{1/3}$ has been used).

To test the new modification to the SB model (section 2), we test two values for the backscatter VMF factor; namely $\text{VMF}_B = 0.05$ and $\text{VMF}_B = 0.5$. $\text{VMF}_B = 0.05$ is close to the minimum permissible value, which corresponds to $\alpha = 0$ in Eq. (3) and implies that $\hat{\phi}_x$ and $\hat{\phi}_z$ are fully independent; this essentially retrieves the (pre-modified) version of the SB model used in O'Neill *et al.* (2015). $\text{VMF}_B = 0.5$ has been chosen partly on empirical grounds; a recent field measurement study of flow within a full-scale isolated street canyon (Blackman *et al.*, 2015) reports a magnitude of $\overline{u'w'}$ of around 1/2 the magnitude of $\sigma_u \sigma_w$ within the roof-level shear layer. By adopting this value, we are thus assuming that the measured ratio is representative of the ratio associated with backscatter in the shear layer, which is not confirmed. However, we also note that $\text{VMF}_B = 0.5$ is close to the maximum permissible value (when $\alpha = 1$) of $\text{VMF}_B \approx 0.6$; the two tested values for VMF_B should therefore also allow us to assess the full extent to which the new modification can affect results.

In summary, we test 12 different configurations of the SB model, corresponding to the 12 possible combinations of: 3 tested values of C_B; 2 tested definitions of l_B; and 2 tested values of VMF_B. This is summarised in Table I.

4. Results and discussion

4.1. Primary eddy intensity

Figure 4 and Figure 5 show normalised profiles of mean vertical velocity, $\bar{w}/\hat{u}$, and mean streamwise velocity, $\bar{u}/\hat{u}$, respectively, for the simulations in Table I and the wind-tunnel experiment, at each of the five across-canyon measurement locations. Here, $\hat{u}$ is the average of $\bar{u}$ between $z/H = 1.0 - 1.5$ over all five locations for any given simulation. An initial inspection suggests that the SB model acts to intensify the primary eddy compared with the Smagorinsky model in all simulations performed, bringing it closer towards that observed in the wind-tunnel experiment, but that the effectiveness of the SB model is rather sensitive to the chosen model parameters. We attempt to quantify the PE intensity from the wind-tunnel experiment and each simulation to aid inter-comparison. Since the time-averaged spanwise velocity component is zero, the mean vorticity field is a 2-D scalar field given by $\omega = \partial_z \bar{u} - \partial_x \bar{w}$. Taking $\bar{u} = \bar{u}(x/W, z/H)$ and $\bar{w} = \bar{w}(x/W, z/H)$, we use the following non-dimensional value as a metric for the PE intensity, ω_{PE}:

$$\omega_{PE} = \frac{1}{\hat{u}} \left(\left[\frac{\bar{u}(0,0.8) - \bar{u}(0,0.1)}{0.7} \right] - \left[\frac{\bar{w}(0.4,0.5) - \bar{w}(-0.4,0.5)}{0.8} \right] \right) \tag{11}$$

Note that the change in $\bar{u}$ is evaluated over a distance of $\Delta z/H = 0.7$, whereas the change in $\bar{w}$ is evaluated over a distance of $\Delta x/W = 0.8$, since no wind-tunnel measurements were taken at $z/H = 0.9$ but were at $z/H = 0.8$. It should be noted that this metric only provides a general indication of the PE intensity; in particular, it is not possible to infer whether certain

regions of the street canyon flow are better simulated (with reference to the wind-tunnel experiment) than others – for this, the 5 spatially distinct vertical profiles should be analysed. The ω_{PE} values for each simulation are given in Table II, both in absolute terms and as a percentage of the wind-tunnel ω_{PE} value. The results confirm that the SB model helps to intensify the PE from that simulated with the Smagorinsky model alone; ω_{PE} is around 30% under-predicted with the Smagorinsky model alone, whereas the inclusion of backscatter can help reduce this discrepancy to as low as 10%, depending on the SB model configuration (discussed later).

Figure 5 also shows that a discrepancy between the wind-tunnel and LES velocity profiles above roof-level ($1 < z/H \leq 1.5$) is largely unaltered by the choice of SGS model (i.e. by the presence or not of backscatter). The wind-tunnel profile shows a steeper gradient nearer $z/H = 1$, indicating a larger amount of mixing in the wind-tunnel free-stream flow than in the LES flow that brings higher-momentum air down towards roof-level. We believe this to be largely attributable to the inclusion of only one explicitly modelled street canyon within the LES domain (due to available computational resources) whereas the wind-tunnel experiment had five street canyons upstream of the test canyon; this limits the size of the largest eddies that can form within the LES free-stream flow compared with in the wind-tunnel experiment. Of course, additional simulations utilising larger computation resources would be required to confirm this. Although the domain size may also explain part of the remaining discrepancy between the wind-tunnel and LES velocity profiles within the street canyon when backscatter is modelled, results from a LES study with 12 explicitly modelled street canyons (Liu and Wong, 2014) suggest that the under-predicted PE intensity cannot be remedied by an increase in domain size alone, reemphasising the importance of the SGS model in this regard.

The fairly wide range of ω_{PE} values in Table II indicates that the effectiveness of the SB model is rather sensitive to the chosen model configuration. To help isolate the effect of each SB model parameter (C_{B}, l_{B} and $\mathrm{VMF}_{\mathrm{B}}$) on the PE intensity, we plot ω_{PE} against each parameter in turn, with one series of points per set of fixed values for the other two parameters. The resulting multi-series plots are shown in Figure 6 (a)-(c), and discussed in turn below.

Backscatter coefficient, C_B

Figure 6(a) shows that increasing C_{B} leads to a monotonic increase in ω_{PE} in 3 of the 4 series. An intensification of the PE with increasing C_{B} might be expected on the presumption that increasing the magnitude of the backscatter fluctuations would act to increase the turbulence flux across the roof-level shear layer, thus increasing the transfer of higher (lower) momentum air into (out of) the street canyon. However, for the simulations using the smaller values of l_{B} and $\mathrm{VMF}_{\mathrm{B}}$ (series CnL1V1), we see that although ω_{PE} initially increases with C_{B} (compare the value at $C_{\mathrm{B}} = 0$, i.e. no backscatter, with the value at $C_{\mathrm{B}} = 0.6$), it then decreases with further increases in C_{B} (although it still remains larger than the value without any backscatter). A proposed explanation for this non-monotonic relationship is as follows. We note that, since the backscatter accelerations have zero mean and (with the current isotropic set-up) random direction, they should act to dissipate any *isolated* coherent structure that they are applied to in favour of randomness (isotropy). Thus, if applied to the *shear-layer alone*, the backscatter accelerations should act to smooth out the sharp velocity gradients within the shear layer, bringing higher momentum flow into the street canyon, which in turn should drive an intensification of the PE. However, if applied to the *primary eddy alone*, the backscatter accelerations should act to reduce the intensity of the primary eddy. (In both cases, an increase in C_{B} would enhance the dissipation of that isolated structure.) Thus, whether the PE intensity increases due to the indirect effect of the backscatter accelerations

on the shear layer or decreases due to the direct dissipative effect of the backscatter accelerations depends on the relative influence of each of these processes. Thus, with the smaller values of l_B and VMF_B selected, it seems that while smaller backscatter accelerations (smaller C_B) favour an intensification of the PE due to the larger (indirect) influence of vertical mixing of the shear layer over the (direct) influence of PE dissipation, larger backscatter accelerations (larger C_B) favour a reduction in PE intensity for the opposite reason. Of course, these arguments should be treated with caution without a more rigorous analysis..

Backscatter length-scale, l_B
Figure 6(b) shows that increasing l_B leads to an intensification of the PE in all the simulations performed. This is rather more expected; larger (in length) backscatter fluctuations will allow higher-momentum flow further above roof-level to be mixed down through the shear layer and into the street canyon, which in turn will drive an intensification of the PE. As the larger tested length-scale gives a simulated PE intensity that is closer to the wind-tunnel PE intensity in all cases tested, we might infer that Eq. (10) is a better measure of the effective grid resolution in our setup than Eq. (9), although this inference should be treated with caution as it is not possible to know what fraction of the PE intensity deficit is attributable to other factors, such as the limited domain size, without further testing.

Backscatter vertical momentum flux factor, VMF_B
Figure 6(c) suggests that the effect of increasing VMF_B on the PE intensity depends on the magnitude of the backscatter accelerations: when $C_B = 0.6$, increasing VMF_B leads to a slight decrease in PE intensity (although it remains larger than the value without any backscatter); when $C_B = 1$, increasing VMF_B does not significantly change the PE intensity, and; when $C_B = 1.4$, increasing VMF_B leads to a significant intensification of the PE – by around 10% of the wind-tunnel PE intensity in one case (series C3L1Vn). Following the same reasoning

as previously discussed, this suggests that with smaller-magnitude backscatter accelerations, an increase in grid-scale VMF enhances the influence of direct dissipation of the PE over the indirect influence of extra vertical mixing across the shear layer, and thus the PE intensity is reduced, whereas with larger-magnitude backscatter accelerations, the opposite is true and so the PE intensifies (with a transition from one regime to the other for intermediate magnitudes).

4.2. Turbulent kinetic energy

Figure 7 shows normalised profiles of mean resolved-scale turbulent kinetic energy (RS-TKE), $\bar{E}/\hat{E}$ for short, for the simulations in Table I and the wind-tunnel experiment, at each of the five across-canyon measurement locations, where $\hat{E}$ is the average RS-TKE between $z/H = 1.0 - 1.5$ over all five locations. We first note that the SB model helps to reduce the spurious RS-TKE bump seen in centre of the street canyon, at $(x/W, z/H) \approx (0,0.5)$, when the Smagorinsky model alone is used. This bump implies that, with the Smagorinsky model, the PE centre has a tendency to move about too much over time. As the backscatter accelerations help to intensify the PE, the additional angular momentum imparted also helps to stabilise it, thus helping to correct this tendency. Other than this, for $C_B \leq 1$, there are no striking differences between the RS-TKE profiles observed with the SB model and with the Smagorinsky model alone, apart from at roof-level where there is a slightly better prediction close to the downstream wall of the street canyon for $C_B = 0.6$, and a slightly worse (over) prediction close to the upstream wall for $C_B = 1$. For $C_B = 1.4$, however, over-predictions at roof-level, and within the upper half of the street canyon close the downstream wall, become more noticeable. Interestingly, however, if we compare the profiles of the two simulations with the larger l_B value (i.e. C3L2V1 and C3L2V2) we see that the *larger* VMF$_B$ value actually helps to *reduce* the over-prediction of RS-TKE; this is particularly noticeable close to the downstream wall, in panels (m)-(o) of the plot. This provides further encouragement

that the new modification to the SB model to increase grid-scale VMF is well-founded. Even with this reduction, however, RS-TKE is still slightly over-predicted in these regions, which suggests that the backscattered energy is perhaps too large with a backscatter coefficient of $C_B = 1.4$. An alternative explanation for this apparent over-prediction might be an issue of scaling in combination with an under-prediction of the large-scale free-stream eddies. We note that with larger RS-TKE values in the region just above roof-level (used for scaling the values within the street canyon) as a result of larger free-stream eddies, the normalised RS-TKE profiles below roof-level would be shifted towards smaller values.

4.3. Shear layer entrainment: Air exchange rate (ACH)

We assess the effect of the SB model on the rate of entrainment through the shear layer by looking at the air exchange rate (ACH). First proposed by Liu *et al.* (2005), the ACH describes the rate of air exchange between the street canyon and the free-stream flow above (units $m^3 s^{-1}$). It thus also provides an assessment of the air ventilation efficiency, with a higher ACH implying a better ventilated street canyon. Continuity dictates that, for an incompressible gas, the volume of air entrained into the street canyon (ACH_+) should be equal to the volume removed from it (ACH_-) over any given period. We may thus calculate ACH at a particular time by integrating only the positive vertical velocities over the street canyon opening, i.e.:

$$ACH_+(t) = \int_{z=H} w_+(t)\, dA, \qquad (12)$$

where $w(t)$ is the instantaneous vertical velocity component at time t, the $+$ subscript implies that only positive values are considered, and A is the area at the top of the street canyon, at $z = H$. Similarly, we can calculate ACH_- by integrating only the negative vertical velocities over the street canyon opening.

The resulting time-averaged values of normalised ACH_+ for each simulation are given in Table II, calculated from the resolved-scale LES fields over a 15-minute period of quasi-steady flow. ACH has been normalised by V/T, where $V = HWL_y$ is the volume of the street canyon within the LES domain, and $T = H/U_{\text{ref}}$ is a time-scale associated with the free-stream flow. Here, we use $U_{\text{ref}} = \bar{u}(z = 1.5H)$ to aid comparison of our results with Liu *et al.* (2005), who used a LES domain height of 1.5H. However, this scaling is somewhat arbitrary, and since ACH has not yet (to our knowledge) been measured by wind-tunnel experiment, the key concern here is the relative differences in ACH among the simulations rather than their exact values. The rate of entrainment through the shear layer is confirmed to be higher with the SB model than with the SMAG model, which is consistent with the observed intensification of the primary eddy within the street canyon. The Smagorinsky model value of $\overline{\text{ACH}_+}/(V/T) = 0.035$ is slightly below the value of 0.05 reported by Liu *et al.* (2005), who used a dynamic SGS model. With the SB model, normalised ACH as much as doubled (0.07 for case C3L2V2), demonstrating that the additional grid-scale fluctuations imparted by the SB model within the roof-level shear layer can cause a significant increase the amount of air entrained into the street canyon from the free-stream flow. The ACH values also illustrate why an increase in the backscatter vertical momentum flux can be effective; comparing runs C3L2V1 and C3L2V2, the time-averaged entrainment rate has been increased by a further 20% (from 0.058 to 0.07), providing the additional momentum needed to drive a further intensification of the primary eddy. A larger backscatter length-scale also increases rate of entrainment; e.g., comparing runs C3L1V1 and C3L2V1, normalised ACH is increased by a further 16% (from 0.05 to 0.058).

5. Conclusions

This study has demonstrated that the use of a stochastic backscatter subgrid-scale model can improve the accuracy of large-eddy simulation of flow within a street canyon. More specifically, for LES of skimming flow within a street canyon of unity aspect ratio, when the approaching wind is perpendicular to the street axis and neutrally stratified, we observed that the SB model could lead to an increase in the intensity of the primary eddy within the street canyon, compared with a simulation using the (purely dissipative) Smagorinsky SGS model alone, thus bringing it significantly closer towards the PE intensity observed in a corresponding (reduced-scale) wind-tunnel experiment. The simulated value of ω_{PE}, a metric for the PE intensity based on the 2-D vorticity field, was increased from approximately 70% of wind-tunnel ω_{PE} value (with the Smagorinsky model alone) to as much as 90% (with the SB model). The additional grid-scale backscatter encourages more turbulent mixing across the roof-level shear layer that separates the PE from the free-stream flow above, thus entraining more momentum into the canyon, which in turn drives an intensification of the PE. An increased rate of entrainment with the inclusion of backscatter was confirmed via calculation of the air exchange rate across the roof-level opening of the street canyon.

Another important contribution of this paper is an improvement to the SB model itself, which allows the backscatter (grid-scale) vertical momentum flux to be increased towards a more appropriate level, based (for example) on empirical observations, whilst still maintaining the appropriate local energy backscatter rate. This modification alone can help to increase simulated value of ω_{PE} by as much as 10% of the wind-tunnel ω_{PE} value, and requires almost no additional computational effort. Furthermore, it was observed that larger grid-scale VMF can help to reduce any over-prediction of resolved-scale turbulent kinetic energy within the upper half of the street canyon.

The sensitivity of the simulated PE intensity to other SB model configuration changes was also investigated; namely, the backscatter coefficient, C_B, and backscatter length-scale, l_B, were both varied. In the simulations performed, larger backscatter fluctuations (larger C_B) typically (but not always) lead to a larger PE intensity, whereas wider backscatter fluctuations (larger l_B) always lead to a larger PE intensity. A measure for the local LES filter length-scale (used to set l_B) based on the maximum of the local grid spacings in each dimension thus gave a better simulated PE intensity than a measure based on the geometric mean of these local grid spacings. The largest tested value of C_B (namely, 1.4) also gave the best match to the wind-tunnel PE intensity, but an over-prediction of RS-TKE in the upper half of the street canyon suggests that this value might be slightly too large. Alternatively, this over-prediction might be a scaling issue resulting from an under-prediction in RS-TKE in the region above roof-level, due to a lack of large-scale eddies in the free-steam flow as a result of the limited size of the modelling domain.

In future work, it would be useful to investigate whether the SB model can also help to improve the prediction of scalar (pollutant) transport and removal from a street canyon in LES-driven dispersion modelling. Efforts should also be made to further improve the generality of the model, which presently requires *a priori* specification of the level of backscatter anisotropy and vertical momentum flux based (typically) on empirical estimates of the grid-scale anisotropy and shear stresses. It may be worth exploring the implementation of a 'dynamic' approach, in which these turbulence properties are evaluated locally at each time step based on the application of an additional test filter and assuming scale similarity.

Appendix A

Derivation of the backscatter stresses, $\overline{u_i' u_j'}_B$

For a continuous backscatter acceleration field, we would have:

$$\boldsymbol{a} = \nabla \times \boldsymbol{\phi} = \begin{bmatrix} \phi_{1,2} - \phi_{2,3} \\ \phi_{1,3} - \phi_{3,1} \\ \phi_{2,1} - \phi_{1,2} \end{bmatrix} \begin{pmatrix} \boldsymbol{i} \\ \boldsymbol{j} \\ \boldsymbol{k} \end{pmatrix}, \tag{A1}$$

where, e.g., $\phi_{1,2}$ denotes the partial derivate of ϕ_1 with respect to y. On the discrete model grid, we have $\boldsymbol{a}^{i,j,k} = \nabla \times \boldsymbol{\phi}^{i,j,k} = \nabla \times g_{i,j,k} \widehat{\boldsymbol{\phi}}^{i,j,k}$,

where sub- and super-scripts i, j and k denote the three discrete model grid-point indices in x, y and z, respectively. Choosing the forward-difference curl operator, and assuming that local gradients in the scaling factor are small, i.e. $\Delta g_{i,j,k} \ll g_{i,j,k}$ for any $\Delta x_i, \Delta y_j, \Delta z_k$, it follows from Eq. (3) that

$$\boldsymbol{a}^{i,j,k} \cong g_{i,j,k} \begin{bmatrix} \left(\alpha \hat{\phi}_1^{i,j+1,k} + \sqrt{1-\alpha^2} \hat{\phi}_3^{i,j+1,k} - \alpha \hat{\phi}_1^{i,j,k} - \sqrt{1-\alpha^2} \hat{\phi}_3^{i,j,k} \right)/\Delta y_j - \left(\hat{\phi}_2^{i,j,k+1} - \hat{\phi}_2^{i,j,k} \right)/\Delta z_k \\ \left(\hat{\phi}_1^{i,j,k+1} - \hat{\phi}_1^{i,j,k} \right)/\Delta z_k - \left(\alpha \hat{\phi}_1^{i+1,j,k} + \sqrt{1-\alpha^2} \hat{\phi}_3^{i+1,j,k} - \alpha \hat{\phi}_1^{i,j,k} - \sqrt{1-\alpha^2} \hat{\phi}_3^{i,j,k} \right)/\Delta x_i \\ \left(\hat{\phi}_2^{i+1,j,k} - \hat{\phi}_2^{i,j,k} \right)/\Delta x_i - \left(\hat{\phi}_1^{i,j+1,k} - \hat{\phi}_1^{i,j,k} \right)/\Delta y_j \end{bmatrix} \begin{pmatrix} \boldsymbol{i} \\ \boldsymbol{j} \\ \boldsymbol{k} \end{pmatrix}, \tag{A2}$$

Each backscatter stress component, $\overline{u_i' u_j'}_B$, can then be obtained from an average of the appropriate product of acceleration components, following Eq. (4). Since the three fields $\hat{\phi}_1$, $\hat{\phi}_2$ and $\hat{\phi}_3$ are uncorrelated with each other, the only non-zero terms after averaging will be those

involving the product of a field with itself. We further recall that each field satisfies $\overline{\widehat{\phi}^2} = 1$, i.e. we have unit variance at any given point. The resulting six components are given by Eq. (5).

References

Baik J-J, Kim J-J. 1999. A numerical study of flow and pollutant dispersion characteristics in urban street canyons. *Journal of Applied Meteorology*. **38**: 1576-1589, doi: 10.1175/1520-0450(1999)038<1576:ANSOFA>2.0.CO;2

Basu S, Porte-Agel F. 2006. Large-eddy simulation of stably stratified atmospheric boundary layer turbulence: A scale-dependent dynamic modeling approach. *Journal of the Atmospheric Sciences*. **63**: 2074-2091, doi: 10.1175/jas3734.1

Blackman K, Perret L, Savory E, Piquet T. 2015. Field and wind tunnel modeling of an idealized street canyon flow. *Atmospheric Environment*. **106**: 139-153, doi: 10.1016/j.atmosenv.2015.01.067

Boppana VBL, Xie ZT, Castro IP. 2010. Large-Eddy Simulation of Dispersion from Surface Sources in Arrays of Obstacles. *Boundary-Layer Meteorology*. **135**: 433-454, doi: 10.1007/s10546-010-9489-9

Brown AR, Derbyshire SH, Mason PJ. 1994. Large-eddy simulation of stable atmospheric boundary-layers with a revised stochastic subgrid model. *Quarterly Journal of the Royal Meteorological Society*. **120**: 1485-1512, doi: 10.1002/qj.49712052004

Brown MJ, Lawson R, Decroix D, Lee R. 2000. Mean flow and turbulence measurements around a 2-D array of buildings in a wind tunnel. In *Proceedings of the 11th Joint AMS/AWMA conference on the applications of air pollution, Long Beach, CA, USA, January 2000.*

Cai XM, Barlow JF, Belcher SE. 2008. Dispersion and transfer of passive scalars in and above street canyons - Large-eddy simulations. *Atmospheric Environment*. **42**: 5885-5895, doi: 10.1016/j.atmosenv.2008.03.040

Chasnov JR. 1991. Simulation of the Kolmogorov inertial subrange using an improved subgrid model. *Physics of Fluids A-Fluid Dynamics*. **3**: 188-200, doi: 10.1063/1.857878

Cheng WC, Liu C-H. 2011. Large-eddy simulation of flow and pollutant transports in and above two-dimensional idealized street canyons. *Boundary-Layer Meteorology*. **139**: 411-437, doi: 10.1007/s10546-010-9584-y

Cheng WC, Porte-Agel F. 2015. Adjustment of Turbulent Boundary-Layer Flow to Idealized Urban Surfaces: A Large-Eddy Simulation Study. *Boundary-Layer Meteorology*. **155**: 249-270, doi: 10.1007/s10546-015-0004-1

Cui ZQ, Cai XM, Baker CJ. 2004. Large-eddy simulation of turbulent flow in a street canyon. *Quarterly Journal of the Royal Meteorological Society*. **130**: 1373-1394, doi: 10.1256/qj.02.150

Deardorff JW. 1970. A numerical study of three-dimensional turbulent channel flow at large Reynolds numbers. *Journal of Fluid Mechanics*. **41**: 453-480, doi: 10.1017/S0022112070000691

Dejoan A, Santiago JL, Martilli A, Martin F, Pinelli A. 2010. Comparison between large-eddy simulation and Reynolds-averaged Navier-stokes computations for the MUST field experiment. Part II: effects of incident wind angle deviation on the mean flow and plume dispersion. *Boundary-Layer Meteorology*. **135**: 133-150, doi: 10.1007/s10546-010-9467-2

Germano M, Piomelli U, Moin P, Cabot WH. 1991. A dynamic subgrid-scale eddy viscosity model. *Physics of Fluids A-Fluid Dynamics*. **3**: 1760-1765, doi: 10.1063/1.857955

Hinze JO. 1972. *Turbulence. 2nd.* McGraw-Hill: USA.

Inagaki A, Castillo MCL, Yamashita Y, Kanda M, Takimoto H. 2012. Large-eddy simulation of coherent flow structures within a cubical canopy. *Boundary-Layer Meteorology*. **142**: 207-222, doi: 10.1007/s10546-011-9671-8

Jeong SJ, Andrews MJ. 2002. Application of the k–ε turbulence model to the high Reynolds number skimming flow field of an urban street canyon. *Atmospheric Environment*. **36**: 1137-1145, doi: 10.1016/S1352-2310(01)00569-6

Kastner-Klein P, Plate EJ. 1999. Wind-tunnel study of concentration fields in street canyons. *Atmospheric Environment*. **33**: 3973-3979, doi: 10.1016/s1352-2310(99)00139-9

Letzel MO, Krane M, Raasch S. 2008. High resolution urban large-eddy simulation studies from street canyon to neighbourhood scale. *Atmospheric Environment*. **42**: 8770-8784, doi: 10.1016/j.atmosenv.2008.08.001

Li X-X, Liu C-H, Leung DYC, Lam KM. 2006. Recent progress in CFD modelling of wind field and pollutant transport in street canyons. *Atmospheric Environment*. **40**: 5640-5658, doi: 10.1016/j.atmosenv.2006.04.055

Lilly DK. 1967. The representation of small-scale turbulence in numerical simulation experiments. *Proceedings of IBM Scientific Computing Symposium on Environmental Sciences*. 195-210

Liu C-H, Wong CCC. 2014. On the pollutant removal, dispersion, and entrainment over two-dimensional idealized street canyons. *Atmospheric Research*. **135**: 128-142, doi: 10.1016/j.atmosres.2013.08.006

Liu CH, Barth MC. 2002. Large-eddy simulation of flow and scalar transport in a modeled street canyon. *Journal of Applied Meteorology*. **41**: 660-673, doi: 10.1175/1520-0450(2002)041<0660:lesofa>2.0.co;2

Liu CH, Leung DYC, Barth MC. 2005. On the prediction of air and pollutant exchange rates in street canyons of different aspect ratios using large-eddy simulation. *Atmospheric Environment*. **39**: 1567-1574, doi: 10.1016/j.atmosenv.2004.08.036

Louka P, Belcher S, Harrison R. 2000. Coupling between air flow in streets and the well-developed boundary layer aloft. *Atmospheric Environment*. **34**: 2613-2621

Mason PJ. 1994. Large-eddy simulation - A critical-review of the technique. *Quarterly Journal of the Royal Meteorological Society*. **120**: 1-26, doi: 10.1002/qj.49712051503

Mason PJ, Brown AR. 1994. The sensitivity of large-eddy simulation of turbulent shear flow to subgrid models. *Boundary-Layer Meteorology*. **70**: 133-150, doi: 10.1007/bf00712526

Mason PJ, Brown AR. 1999. On subgrid models and filter operations in large eddy simulations. *Journal of the Atmospheric Sciences*. **56**: 2101-2114, doi: 10.1175/1520-0469(1999)056<2101:osmafo>2.0.co;2

Mason PJ, Callen NS. 1986. ON THE MAGNITUDE OF THE SUBGRID-SCALE EDDY COEFFICIENT IN LARGE-EDDY SIMULATIONS OF TURBULENT CHANNEL FLOW. *Journal of Fluid Mechanics*. **162**: 439-462, doi: 10.1017/s0022112086002112

Mason PJ, Thomson DJ. 1992. Stochastic backscatter in large-eddy simulations of boundary-layers. *Journal of Fluid Mechanics*. **242**: 51-78, doi: 10.1017/s0022112092002271

O'Neill JJ, Cai X-M, Kinnersley R. 2015. A generalised stochastic backscatter model: large-eddy simulation of the neutral surface layer. *Quarterly Journal of the Royal Meteorological Society*. Advance online publication, doi: 10.1002/qj.2548

Oke TR. 1987. *Boundary Layer Climates. Second Edition.* Methuen: London, UK.

Palmer T, Buizza R, Doblas-Reyes F, Jung T, Leutbecher M, Shutts G, Steinheimer M, Weisheimer A. 2009. *Stochastic Parametrization and Model Uncertainty. ECMWF Technical Memorandum 598.* European Centre for Medium-Range Weather Forecasts: Reading, UK.

Park SB, Baik JJ. 2013. A Large-Eddy Simulation Study of Thermal Effects on Turbulence Coherent Structures in and above a Building Array. *Journal of Applied Meteorology and Climatology*. **52**: 1348-1365, doi: 10.1175/jamc-d-12-0162.1

Pavageau M, Schatzmann M. 1999. Wind tunnel measurements of concentration fluctuations in an urban street canyon. *Atmospheric Environment*. **33**: 3961-3971, doi: http://dx.doi.org/10.1016/S1352-2310(99)00138-7

Pielke R, Cotton W, Walko Rea, Tremback CJ, Lyons WA, Grasso L, Nicholls M, Moran M, Wesley D, Lee T. 1992. A comprehensive meteorological modeling system—RAMS. *Meteorology and Atmospheric Physics*. **49**: 69-91

Piomelli U, Balaras E. 2002. Wall-layer models for large-eddy simulations. *Annual Review of Fluid Mechanics*. **34**: 349-374, doi: 10.1146/annurev.fluid.34.082901.144919

Salim SM, Buccolieri R, Chan A, Di Sabatino S. 2011a. Numerical simulation of atmospheric pollutant dispersion in an urban street canyon: Comparison between RANS and LES. *Journal of Wind Engineering and Industrial Aerodynamics*. **99**: 103-113, doi: 10.1016/j.jweia.2010.12.002

Salim SM, Cheah SC, Chan A. 2011b. Numerical simulation of dispersion in urban street canyons with avenue-like tree plantings: Comparison between RANS and LES. *Build. Environ.* **46**: 1735-1746, doi: 10.1016/j.buildenv.2011.01.032

Salizzoni P, Soulhac L, Mejean P. 2009. Street canyon ventilation and atmospheric turbulence. *Atmospheric Environment*. **43**: 5056-5067, doi: 10.1016/j.atmosenv.2009.06.045

Santiago JL, Dejoan A, Martilli A, Martin F, Pinelli A. 2010. Comparison Between Large-Eddy Simulation and Reynolds-Averaged Navier-Stokes Computations for the MUST Field Experiment. Part I: Study of the Flow for an Incident Wind Directed Perpendicularly to the Front Array of Containers. *Boundary-Layer Meteorology*. **135**: 109-132, doi: 10.1007/s10546-010-9466-3

Schumann U. 1975. Subgrid scale model for finite difference simulations of turbulent flows in plane channels and annuli. *Journal of Computational Physics*. **18**: 376-404, doi: 10.1016/0021-9991(75)90093-5

Shutts G. 2005. A kinetic energy backscatter algorithm for use in ensemble prediction systems. *Quarterly Journal of the Royal Meteorological Society*. **131**: 3079-3102, doi: 10.1256/qj.04.106

Smagorinsky J. 1963. General circulation experiments with the primitive equations. *Monthly Weather Review*. **91**: 99-164, doi: 10.1175/1520-0493(1963)091<0099:gcewtp>2.3.co;2

Tominaga Y, Stathopoulos T. 2010. Numerical simulation of dispersion around an isolated cubic building: Model evaluation of RANS and LES. *Build. Environ.* **45**: 2231-2239, doi: 10.1016/j.buildenv.2010.04.004

Walton A, Cheng AYS. 2002. Large-eddy simulation of pollution dispersion in an urban street canyon - Part II: idealised canyon simulation. *Atmospheric Environment*. **36**: 3615-3627, doi: 10.1016/s1352-2310(02)00260-1

Weinbrecht S, Mason PJ. 2008. Stochastic backscatter for cloud-resolving models. Part I: Implementation and testing in a dry convective boundary layer. *Journal of the Atmospheric Sciences*. **65**: 123-139, doi: 10.1175/2007jas2166.1

Xie Z, Voke P, Hayden P, Robins A. 2004. Large-Eddy Simulation of Turbulent Flow Over a Rough Surface. *Boundary-Layer Meteorology*. **111**: 417-440, doi: 10.1023/b:boun.0000016599.75196.17

Xie ZT, Castro IP. 2006. LES and RANS for turbulent flow over arrays of wall-mounted obstacles. *Flow Turbulence and Combustion*. **76**: 291-312, doi: 10.1007/s10494-006-9018-6

Zidikheri MJ, Frederiksen JS. 2009. Stochastic subgrid parameterizations for simulations of atmospheric baroclinic flows. *Journal of the Atmospheric Sciences*. **66**: 2844-2858, doi: 10.1175/2009jas3036.1

Tables

Table I – Configuration of SB model for each LES run. C_B is the backscatter coefficient, l_B the backscatter length-scale, and VMF_B the backscatter VMF factor. SMAG refers to a run that uses the Smagorinsky SGS model alone (i.e. no backscatter).

Run Name	C_B	l_B	VMF_B
SMAG	N/A	N/A	N/A
C1L1V1	0.6	Eq. (9) used	0.05
C1L1V2	0.6	Eq. (9) used	0.5
C1L2V1	0.6	Eq. (10) used	0.05
C1L2V2	0.6	Eq. (10) used	0.5
C2L1V1	1.0	Eq. (9) used	0.05
C2L1V2	1.0	Eq. (9) used	0.5
C2L2V1	1.0	Eq. (10) used	0.05
C2L2V2	1.0	Eq. (10) used	0.5
C3L1V1	1.4	Eq. (9) used	0.05
C3L1V2	1.4	Eq. (9) used	0.5
C3L2V1	1.4	Eq. (10) used	0.05
C3L2V2	1.4	Eq. (10) used	0.5

Table II – Primary eddy intensity, ω_{PE}, and normalised air exchange rate ($\overline{ACH_+}$) for the wind-tunnel (WT) experiment and each LES run. (Note that $\overline{ACH_+}$ was not calculated in the WT experiment).

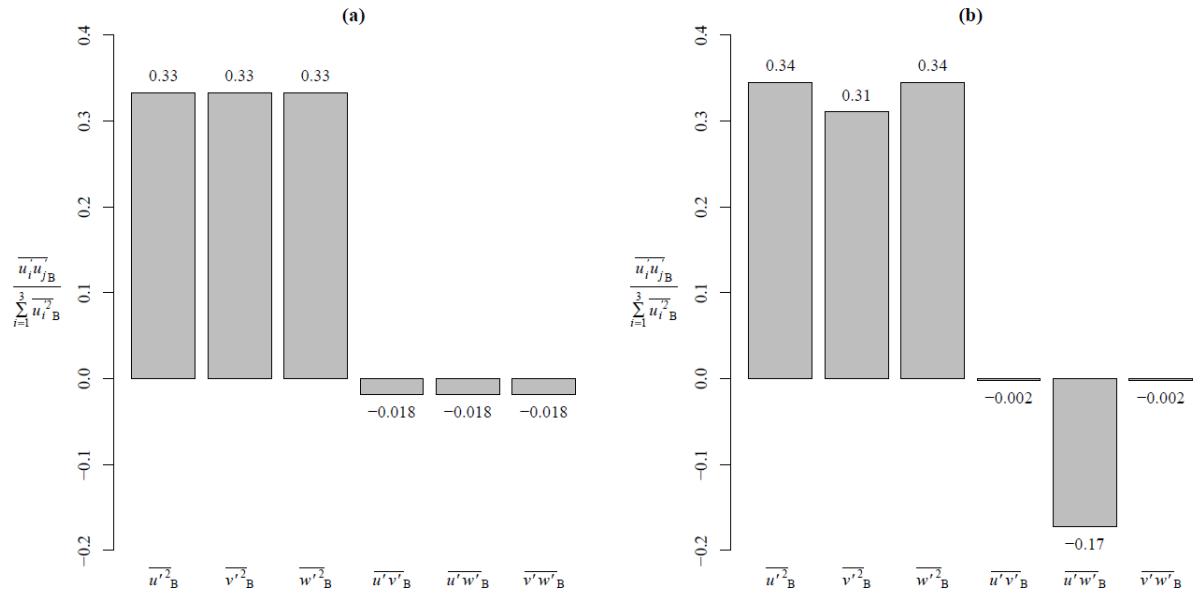| Case	ω_{PE}	% of WT ω_{PE}	$\overline{ACH_+}/(V/T)$
WT	2.56	100	N/A
SMAG	1.75	69	0.035
C1L1V1	1.90	74	0.043
C1L1V2	1.85	72	0.044
C1L2V1	1.94	76	0.047
C1L2V2	1.92	75	0.046
C2L1V1	1.85	72	0.046
C2L1V2	1.85	72	0.044
C2L2V1	2.05	80	0.051
C2L2V2	2.04	80	0.054
C3L1V1	1.78	70	0.050
C3L1V2	2.06	81	0.056
C3L2V1	2.10	82	0.058
C3L2V2	2.28	89	0.070

Figure Captions

Figure 1 – Normalised backscatter stresses on an isotropic model grid with resolution Δ and a backscatter length-scale of $l_B = \Delta$, with a backscatter VMF factor of (a) $VMF_B = 0.05$ (corresponds to $\alpha = 0$), and (b) $VMF_B = 0.5$ (corresponds to $\alpha = 0.89$).
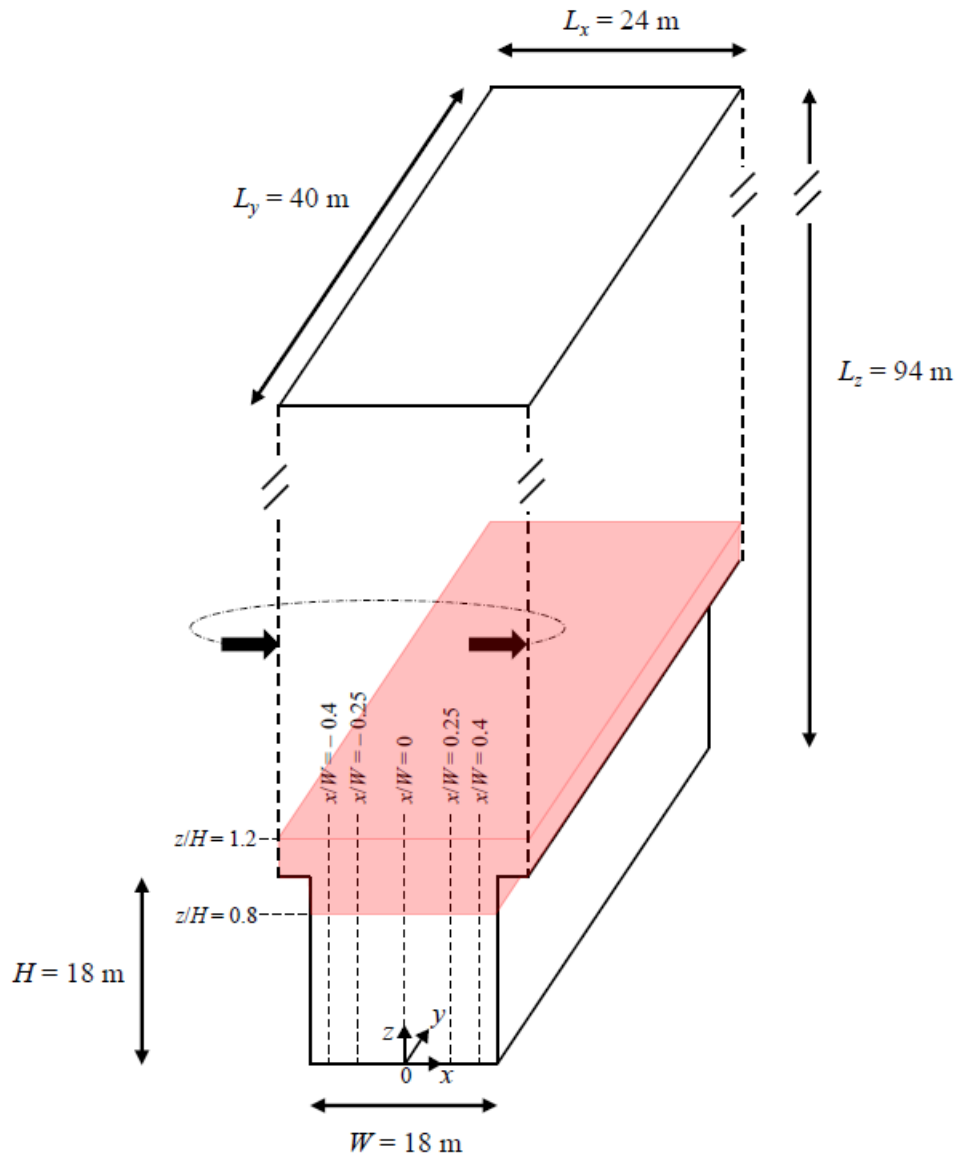
Figure 2 – Dimensions of the LES computational domain. Vertical dashed lines within the street canyon show the five transects along which time-averaged statistics are computed for comparison with the wind-tunnel data. Periodic boundary conditions are used in x (above roof-level) and y. The shaded region shows where the backscatter accelerations are added to the LES field.
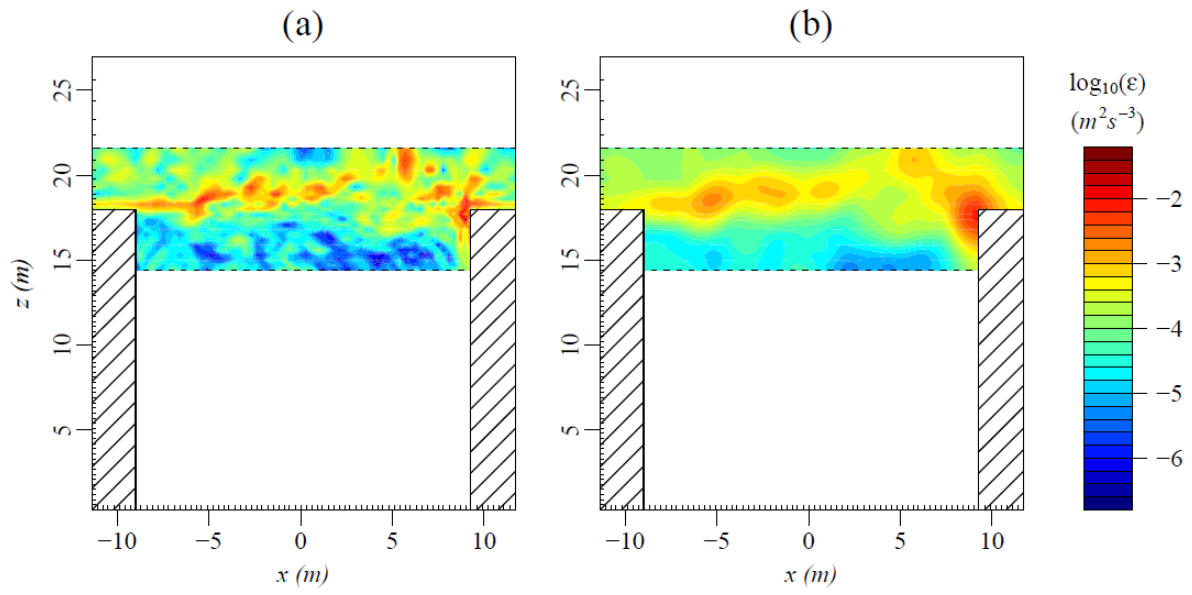
Figure 3 – An x-z contour slice of the logarithm (base 10) of an instantaneous dissipation field, for the area of the domain in which backscatter accelerations are added, with: (a) no filter applied; (b) the SB model filter applied, as done before calculating the point-wise energy backscatter rates.
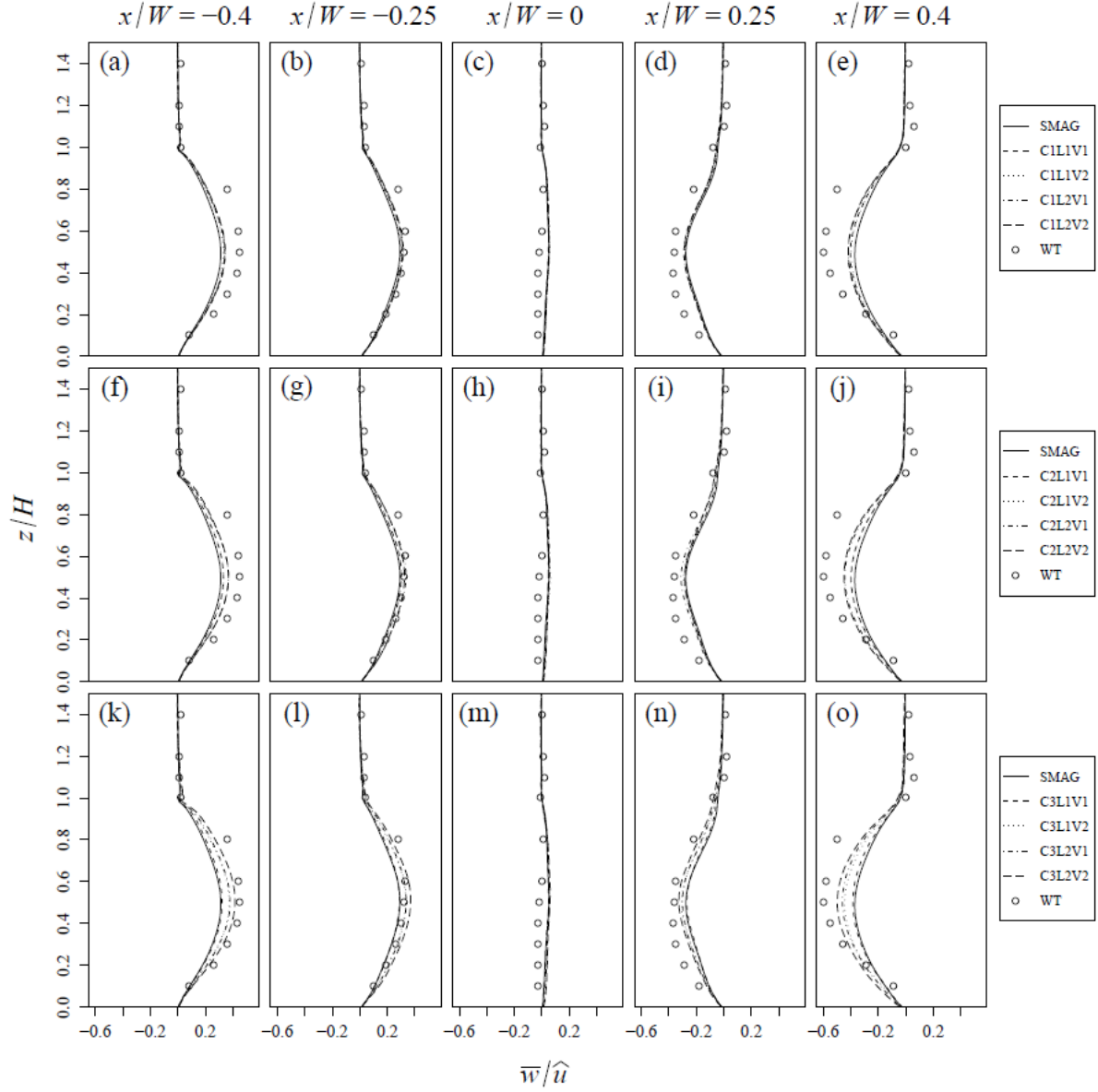
Figure 4 – Normalised profiles of mean vertical velocity, $\bar{w}/\hat{u}$, at locations (from left to right) $x/H = -0.4, -0.25, 0, 0.25, 0.4$, respectively. Circles show wind-tunnel data and curves show LES results: solid black lines – Smagorinsky model only; short-dashed lines – smaller l_B and VMF_B values; dotted lines – smaller l_B value, larger VMF_B value; dot-dash lines – larger l_B value, smaller VMF_B value; long-dashed lines – larger l_B and VMF_B values. Top row (panels (a)-(e)) $- C_B = 0.6$; middle row (panels (f)-(j)) $- C_B = 1.0$; bottom row (panels (k)-(o)) $- C_B = 1.4$.
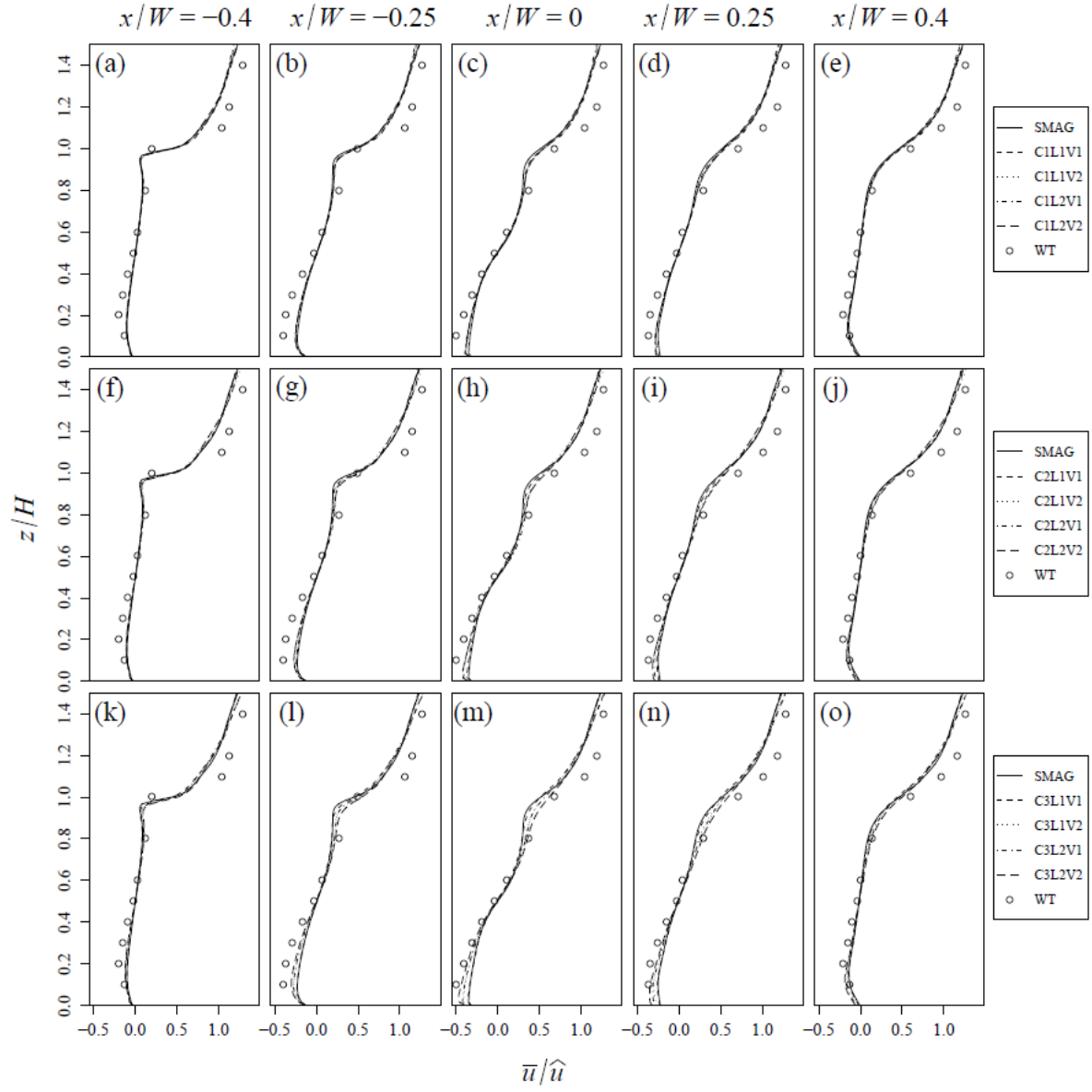
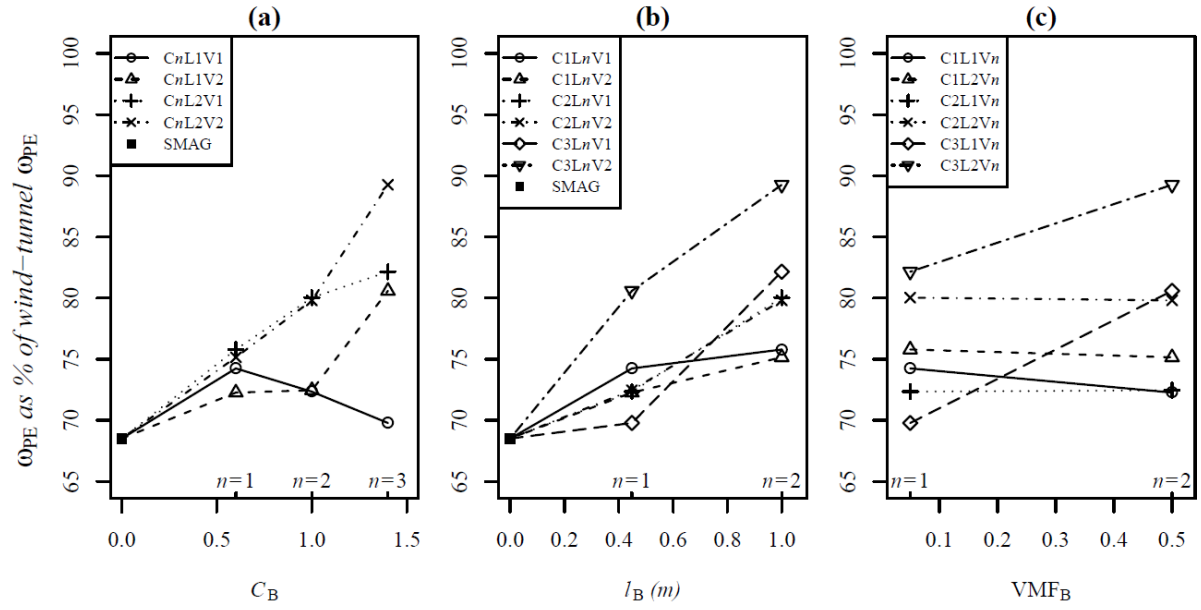**Figure 5 – Same as in Figure 4 but for normalised profiles of mean streamwise velocity,** $\overline{u}/\widehat{u}$.

Figure 6 – Multi-series line plots of ω_{PE} (as a % of ω_{PE} from the wind-tunnel experiment) versus (a) C_B, (b) l_B, (c) VMF$_B$. Each series shows a set of runs for which the main parameter varies whilst other two parameters are held fixed. The value of n on the lower axis should be inserted into the relevant legend entry to give the corresponding run name (see Table I). Note that in panel (b), $l_B = 0.45$ m refers to the value of $\left(\Delta x_i \Delta y_j \Delta z_k\right)^{1/3}$ within the street canyon (i.e. below roof level), where $\Delta x, \Delta y, \Delta z = 0.3$ m, 1 m, 0.3 m are fixed.
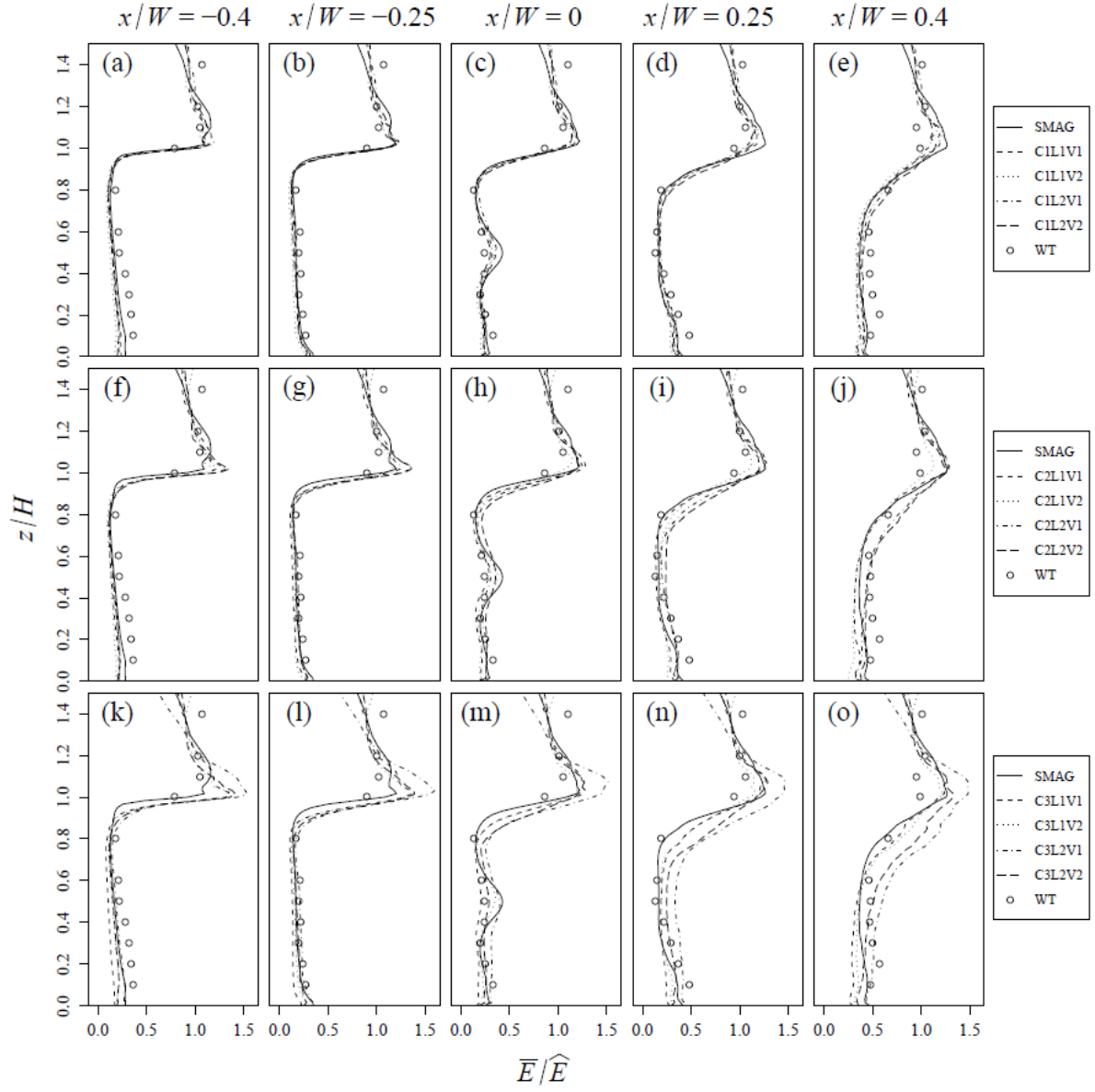
Figure 7 – Same as in Figure 4 but for normalised profiles of resolved-scale turbulent kinetic energy, $\overline{E}/\widehat{E}$.